Characters of neoantigens in cancer immunotherapy

Peng Bai[1], Yongzheng Li[1], Qiuping Zhou[1], Jiaqi Xia[1], Min Wu[2], Sanny K. Chan[3,4,5], John W. Kappler[3,6,7,8], Yu Zhou[1], Philippa Marrack[3,6,9], Lei Yin[1]

1 State Key Laboratory of Virology, Hubei Key Laboratory of Cell Homeostasis, College of Life Sciences, Wuhan University, Wuhan, 430072, Hubei, China

2 Hubei Key Laboratory of Cell Homeostasis, College of Life Sciences, Wuhan University, Wuhan, 430072, Hubei, China

3 Department of Biomedical Research, National Jewish Health, Denver, CO 80206, USA

4 Department of Pediatrics, University of Colorado Denver School of Medicine, Aurora, CO 80045, USA

5 Division of Pediatric Allergy-Immunology, National Jewish Health, Denver, CO 80206, USA

6 Barbara Davis Center for Childhood Diabetes, University of Colorado, Aurora, CO 80045, USA

7 Department of Immunology and Microbiology, University of Colorado School of Medicine, Aurora, CO 80045, USA

8 Structural Biology and Biochemistry program, University of Colorado Anschutz Medical Campus, Aurora, CO 80045, USA

9 Department of Biochemistry and Molecular Genetics, University of Colorado Anschutz Medical Campus, Aurora, CO 80045, USA

Abstract

Evidences have suggested that T cells that target mutation derived neoantigens are the main mediators of many effective cancer immunotherapies. Although algorithms have been used to predict neoantigens, only a handful of those are truly immunogenic. It is unclear which other factors influence neoantigen immunogenicity. Here, we classified clinical human neoantigen/neopeptide data based on their peptide-MHC binding events into three categories. We observed a conserved mutation orientation in anchor mutated neoantigen cohort after classification. By integrating this rule with existing prediction algorithm, we achieved improved performance of neoantigen prioritization. We solved several neoantigen/MHC structures, which showed that neoantigens which follow this rule can not only increase peptide-MHC binding affinity but create new TCR binding features. We also found neoantigen exposed surface area may lead to TCR bias in cancer immunotherapy. These evidences highlighted the value of immune-based classification during neoantigen study and enabled improved efficiency for cancer treatment.

Keywords: cancer immunology; major histocompatibility complex (MHC); vaccine; neoantigen prediction; antigen immunogenicity

Introduction

The immune system can sometimes recognize and destroy cancer cells[1]. $CD8^+$ T cells are a major component in this process by both recognizing and destroying the target cells[2–5]. For T cells to react with tumor cells two components are required: major histocompatibility complex class I and possibly class II proteins (MHCI, MHCII) on the cancer cells and tumor derived antigenic peptides which bound to MHCs. T cells can then recognize such complexes, called pMHC epitopes (the combination of MHC and antigen), on the cancer cells as abnormal cells and target them for destruction. Thus, it is crucial to identify cancer antigens for immunotherapy.

During the last 25 years, great efforts have been made to identify tumor antigens[6]. These tumor antigens can be classified into two broad categories, self-antigens which are seldom expressed in normal tissues or expressed at much higher levels on the cancer cell versus normal tissues (like

NY-ESO-1, MART-1) and nonself-antigens called neoantigens which are derived from somatic mutations in cancer cells[7]. Neoantigens are not presented by normal tissues, hence the immune system is not tolerant to them and views them, correctly, as foreign antigens and responds appropriately[8,9].

Currently, neoantigen identifying methods relies on next-generation sequencing (NGS) to provide formidable identification of cancer mutations, followed by predicting their theoretical binding for the patient's HLA complex[10–14][15,16]. In brief, they compared tumor and normal DNA for identifying non-synonymous mutations and used peptide/MHCI binding prediction algorithms to find mutated peptides which could bind MHC to be potential effective neoantigens. Binding prediction could lighten the burden of immunotherapy by reducing the number of candidate neopeptides[7,10,12,16–19,19–22,22–25]. However, among neoantigens with actual MHC binding, only a small portion of them are immunogenic and have therapeutic effects[26,27]. It is likely that other features beyond MHC binding affinity could affect neoantigen immunogenicity.

It has been hypothesized that the TCR:pMHC ternary binding events may influence neoantigen immunogenicity. Yadav *et al*. and Fritsch *et al*. suggested that the side chain of neoantigen mutation point towards the T-cell receptor (TCR) would be more immunogenicity while Duan *et al*. thought that neoantigen substitutions at MHC anchor positions may be more important[7,18,28]. Recently, Capietto *et al.* also suggested that the MHC binding affinity of neoantigen corresponding wild type peptide is associated with predicting cancer neoantigens, with their mouse model study[29]. However, studies in this area are still limited due to scarce large human neoantigen datasets and neoepitope structures availability. Thus, systematic analyses based on large human neoantigen data and structural understanding of neoantigen immune properties are still needed.

Here, we attempted to determine different features between immunogenic neoantigens and noneffective neopeptides after mutation positional classification of human clinical neoantigens. We found that almost all immunogenic anchor mutated neoantigens in our datasets followed a unique mutation pattern (termed NP rule), rather than other patterns. Combining this rule with existing binding predictor could improve the neoantigen prioritization performance.

To provide structural insights of neoantigens with the NP rule, we solved several pMHC structures which follow this rule: the driver mutation derived KRAS G12D neoantigens in complex with

HLA-C*08:02 and the noneffective mouse DPAGT1 peptides in complex with mouse MHC H-2 Kb. We showed that neoantigens which follow the NP rule could generate new immune features for T cell recognition. The newly generated surface is necessary for anchor mutated cancer peptides to induce T cell response *in vivo*. It also suggested that the antigen exposed surface area might be an additional factor involves in neoantigen immunogenicity.

Results

Classification of cancer neoantigen/neopeptide data by mutation position

To study immune features of clinically relevant neoantigens arising from cancer mutations, we obtained HLA-I immunogenic (positive data, termed neoantigen) and noneffective (negative data, termed neopeptide) human clinical cancer neoantigen/neopeptide data from our NEPdb database (unpublished). These data come from 34 papers which contain neoantigen/neopeptide sequences and relevant HLAs as well as *in vitro* T cell assay reports and clinical tests[5,30,10–12,16,21,31–41,17,42,43,19,44–49,22,50–52].

The Immunogenic Neoantigen Dataset (IND) in this study, contains 128 entries (Fig. 1a; Supplementary Table 1). Neoantigens without T cell assay, minimal length or relevant HLA information were not recorded in the IND datasets. Melanoma and non-small cell lung cancer, with higher mutational burdens and more extensively studies, contained nearly 80% entries in this dataset.[24].

In this study, 11739 noneffective neopeptides with corresponding MHCIs formed the Raw Noneffective Neopeptide Dataset (RNND) (Fig. 1a; Supplementary Table 2). All of these mutant peptides had been tested by T cell assays at least or tested in clinical trials, which were proven to be noneffective. The majority of them are not minimal peptides lengths (MHCI bind peptides that are predominantly 8-11 amino acid in length) known to present by MHCI. As we know, peptide-MHC binding is necessary albeit not sufficient for neoepitope immunogenicity. To process noneffective neopeptides into optimal length (9mer and 10mer) as negative control for further study, we used the NetMHCpan 4.0 algorithm for peptide-MHC binding prediction. This processed dataset is termed Noneffective Neopeptide Dataset (NND) and contains 2883 entries (Fig. 1a; Supplementary Table 3).

Neoantigen with strong binding affinity to MHC can form stable pMHC complex for T cell recognition and therefore induce T cell responses. Thus, neoepitope candidates could be prioritized through prediction algorithms to eliminate those peptides with weak binding affinity to MHCI. While the binding prediction algorithms have used for eliminating candidate neoantigens, the prediction accuracy of neoantigens capable of eliciting efficacious antitumor responses in patients remains quite low[53]. It is likely that features beyond MHC binding affinity involve in neoantigen immunogenicity. Recently, some studies found that the TCR:pMHC ternary binding events may influence immunogenicity[54,55]. However, the underlying immunological mechanisms of how the positional mutations affect cancer clinical outcome remains poorly defined.

In an attempt to answer above questions, we classified peptides from IND and NND based on the mutation position. To be specific, peptides from IND and NND were categorized into three categories: mutated at an anchor position (binds MHC intensively), MHC-contacting position (contacts MHC but provides less binding affinity) and TCR-contacting position (point towards TCR instead of MHC). The classification was performed by referencing the SYFPEITHI database[56], NetMHCpan antigen binding motif [24] and the Protein Data Bank (PDB) pMHC structures into account (see Methods). The classified information was recorded in Supplementary Table 1 and Supplementary Table 3.

We next calculated the percentage of neoantigens in different categories after classification. Immunogenic neoantigens were more likely to mutate at TCR-contacting region (Fig. 1b, c) and were less likely to change at MHC-contacting regions than those noneffective neopeptides (Fig. 1b, c). These results suggested that neopeptides with TCR-contacting position mutation rather MHC-contacting position will preferentially be immunogenic[7,28]. However, the percentage of anchor mutated neoantigens did not show significant differences compared with noneffective neopeptides (Fig.1c). It suggested that classification of anchor mutated peptides is not sufficient to distinguish immunogenic neoantigen from noneffective neoantigen candidates.

Anchor mutated neoantigens followed a conservative mutation pattern to acquire immunogenicity

We aimed to further characterize the intrinsic immunological properties of anchor mutated neoantigens beyond binding affinity. MHC molecules have many allelic variants with different binding properties of

their peptide binding cleft. Thus, the peptides recognized by different MHCs are very diverse, with allele-specific amino acid preferences. To investigate the preferential property of the anchor mutated peptide and its wild type counterparts in the context of HLAs, we set the cut-off frequency to be above 10% as HLA preferential amino acids at anchor positions as described previously[57] based on large peptide binding datasets from the IEDB[58] (Supplementary Fig. 1, Supplementary Table 1 and 3). With the definition of "preference", the anchor mutated neopeptide pairs (contain wild-type and mutant peptides) can be divided into 4 groups : non-preferential to non-preferential residues (mutated from wild-type counterparts with non-preferential amino acid to mutation with non-preferential amino acid, within the context of the certain HLA, abbreviated as NN), non-preferential to preferential residues (NP), preferential to non-preferential residues (PN) and preferential to preferential residues (PP) (Fig. 1d; Supplementary Table 4). Statistical analysis showed that the frequency of the immunogenic pairs with NP preferential change was significantly higher than those from the noneffective pairs (Fig. 1d, p=8.247e-06). Almost all (26 in 27) of the immunogenic pairs (from IND) appear to be classified into the NP group. In contrast, cancer neopeptides with HLA non-preferential property (the NN or PN groups) or those wild-type counterparts with HLA preferential property (the PN or PP groups) can hardly induce effective anti-tumoral response (Fig. 1e; Supplementary Table 4).

Next, we checked the exceptional case (the one which did not follow the NP rule in 27 cases). This neoantigen (MYADM R30W) from the MYADM protein has a mutation at C termini of the peptide that changes Arg to Trp. Of note, both wild type and mutant MYADM peptides can elicit self T cell responses[31]. This evidence suggested that, in this case, wild type peptide can also bind the patient's HLA protein and eliciting T cell autoreactivity *in vivo*. Since both the MYADM neoantigen and its wild-type counterpart were reactive in this patient, this antigen should be excluded for further use. Notwithstanding this exception, our observations suggested the NP rule of anchor mutated neoantigens is a conservative feature to assess T cells for reactivity against neoepitopes.

The NP rule of anchor mutated neoantigens thus can be treated as a binary variable (1= true NP, 0= false NP). To assess whether this variable can be used in neoantigen candidate prioritization, we tested the performance of the binary "NP" model and the combination model of the binary "NP" model with NetMHCpan 4.0 Rank% model (termed Com NP+B). Two existing prediction models, the NetMHCpan 4.0 (using NetMHCpan 4.0 Rank% score) and the DAI models (differential agretopic index, the difference of predicted binding affinity between the mutated epitope and its unmutated counterpart)

were also tested with our data as benchmark comparators. After taking the NP rule into account, the "Com NP+B" model achieved better performance compared with other three models (Fig. 1f, AUC=0.810). When comparing the performance of the four predictors, assessment was also done by 50-fold cross-validation (2/3rd random resampling) over the data to check whether the observed difference in average AUC differs significantly (Supplementary Fig. 2). Collectively, we proved that the NP rule can be taken as a predictive feature to improve neoantigen candidate prioritization.

Anchor mutated neoantigens can generate new surface for T cell recognition

Our results above indicated that the NP rule is a conservative feature in the immunogenic anchor mutated neoantigens. To understand how this rule forms the basis for acquired immunogenicity of anchor mutated neoantigens, we attempted to solve the structures of the typical neoepitopes: HLA-C*08:02 (C08) in complex with KRAS mutation derived neoantigens form a successful clinical case, reported by Tran *et al*[10]. In this case, objective regression of metastases was observed in a metastatic colorectal cancer patient after the infusion of HLA-C*08:02-restricted tumor-infiltrating lymphocytes (TILs) targeting KRAS G12D neoantigens. The KRAS G12D mutant 9mer peptide GA<u>D</u>GVGKSA and 10mer peptide GA<u>D</u>GVGKSAL (both mutated at position 3 from glycine to aspartic acid) can stimulate autologous HLA-C*08:02 reactive T cells, while their wild-type counterparts cannot[10]. These two neoantigens can be categorized in the anchor mutated group (Supplementary Table 1 and reference[59]) and follow the NP rule.

First, we attempted to get the protein complexes of HLA-C*08:02 (C08) in complex with four peptides: wild type KRAS 9mer GAGGVGKSA (wt9m); wild type KRAS 10mer peptide GAGGVGKSAL (wt10m); mutant KRAS G12D 9mer peptide GA<u>D</u>GVGKSA (mut9m, mutation site is indicated with underline) and mutant KRAS G12D 10mer peptide GA<u>D</u>GVGKSAL (mut10m). C08-mut9m and C08-mut10m complexes were successfully refolded. However, C08-wt9m complex and C08-wt10mer complex failed to refold even with ten-fold increase in concentration of the peptides. This result confirmed that the mutation from glycine to aspartic acid of these neoantigens is crucial to stabilize pMHC complex.

We next solved the C08-mut9m complex at 2.4 angstroms (Å) and the C08-mut10m complex at 1.9 Å (Supplementary Table 5). The electron density at the peptide region was unambiguous (Fig. 2a, b). The

C08-mut9m complex and the C08-mut10m complex showed a conserved conformation except the peptide region (Fig.2c, d). The smaller residues such as alanine and serine are preferably selected at peptide P1 and P2 position by the peptide binding motif of HLA-C*08:02 (Fig.2e, Supplementary Fig. 1). This is due to the narrow cleft formed by several C*08:02 aromatic residues (Tyr7, Phe33, Tyr67, Tyr99, Tyr59, Tyr171, Tyr159 and Trp167) which limits the size of the P1 and P2 side chains that can bind at that site (Fig.2f).

Generally, peptides use anchor positions at P2 and PΩ to occupy the B and F pockets of HLA class I molecules. However, the structures of the C08-mut9m and C08-mut10m, followed by the peptide binding analysis, revealed that KRAS G12D 9mer and 10mer peptides use unconventional P3 and PΩ sites as anchors to form stable complexes with HLA-C*08:02 (Fig. 2g, h; Supplementary Fig. 1). The B pocket of HLA-C*08:02 bind P3D via interactions with Arg97 and Arg156. The P3D side chain of C08-mut9m also forms an intra-chain hydrogen bond with P4G, while this hydrogen bond is absent in the C08-mut10m structure. Interestingly, it is apparent from the C08-mut9m structure that the anchor residue P3D could also provide TCR accessible surface by partially exposing of its charged side chain (Supplementary Fig. 3). This unusual phenomenon suggested that anchor mutation of some neoantigens can not only improve pMHC binding force but could also provide additional accessible surface for TCR interaction, under certain conditions, and therefore change the total strength of the TCR:pMHC complex.

At the PΩ anchor position, although the 9mer and 10mer peptides occupied the same F pocket with their PΩ residues, the P10L side chain from the 10mer peptide is buried more deeply than P9A in the 9mer structure (Fig. 2g, h). Meanwhile, instead of the upward residue P8S in mut9m peptide, the mut10m peptide uses P8S as an auxiliary anchor to bind the HLA protein via hydrogen bonds to Glu152 and Arg156. These interactions from the mut10m squeezed the P4 to P7 residues together with residue P3D (Fig. 2h). Although the mut9m and the mut10m have similar sequences with only one amino acid different at PΩ termini, the surface details are largely different after they engage with HLA-*08;02. We postulated that these different features from the mut9m and mut10m neoepitopes may respectively modulate the effective T cell recognition and activate different T cell repertoires (discussed below).

Noneffective anchor mutated neoantigens could not generate more differentiated TCR binding surface

than their wild-type analogues, as they buried the anchor mutations into MHC pocket and can hardly contact with TCRs. However, structural analysis of immunogenic anchor mutated neoantigens suggested that these neoantigens can not only generate new immune features, but even create novel neoepitope surface. Thus, the necessity and conservation of NP rule in anchor mutated neoantigen might be explained by the generation of novel surface from mutant peptide, rather than the wild-type analogue, which could enable the boosting of neoepitope-specific response from T cells.

Structural of non-therapeutic mouse neoantigen DPAGT1 V213L in complex with H-2 Kb

We next determined two structures of non-immunogenic neopeptides with anchor mutation. Yadav *et al* described a neopeptide that can be presented by MHC but showed non-immunogenic property *in vivo*[7]. This mouse DPAGT1 V213L neopeptide contains a mutated C-terminal anchor residue that falls into the “preferential to preferential residues (PP)” group, with the changing of valine(V) to leucine(L).

Soluble mouse H-2 Kb in complex with mutant DPAGT1 V213L 8mer peptide (SIIVFNLL, termed mut8mL) and the wild type 8mer counterpart (SIIVFNLV, termed wt8mV) were separately expressed, refolded and purified for crystallization trials. Crystal diffraction data of Kb-wt8mV and Kb-mut8mL were processed to 2.4 Å and 2.5 Å resolution respectively (Supplementary Table 5) and provided electron density for each peptide (Fig. 3a).

The overall structure of the Kb-wt8mV complex closely resembles that of Kb-mut8mL with the exception of a slight difference at PΩ (P8) (Fig. 3b). The C-terminal PΩ residue acted as an anchor in both the Kb-wt8mV and the Kb-mut8mL complexes (Fig. 3b). Moreover, both PΩ valine and leucine were preferably selected by H-2 Kb (Fig. 3c). Both of the two PΩ residues formed hydrogen bonds with Kb Asp77, Tyr84, Thr143 and Lys146 (Fig. 3d, e). Although the side chain of leucine in the mut8mL peptide inserted more deeply into Kb than valine in the wt8mV peptide because of its longer side chain, these two peptides did not provide different TCR binding surface with relevant MHCs (Fig. 3b, d, e). These findings indicated that neopeptides with the “PP” rule cannot readily change the binding surface and therefore immunogenicity. The non-effectiveness across the neopeptides with PP rule might be explained by the pre-existence of the wild-type peptide-MHC complex in thymus, which can lead to negative selection of potential neopeptide restricted T cell repertoires. Considering that

peptide-MHC binding is necessary for neoepitope immunogenicity, we did not further discuss the situation of those neopeptides with the “PN” or the “NN” rule.

Neoantigen exposed surface areas may affect T cell selection in cancer immunotherapy

Peptide antigen can form stable complexes with HLA by lying the peptide chain into the HLA antigen-binding cleft. Some antigens, called “featureless” antigens, have relatively small exposed surface areas (ESA) form side chains pointing towards the T cell receptor when they fill the peptide-binding cleft of HLAs[60]. Studies have indicated that featureless epitope are more likely to select relatively narrow TCR repertoires than epitopes with large exposed features *in vivo*[61]. We next examined the ESA features of the C08-mut9m and the C08-mut10m structures, by employing the PDBePISA server. Of note, the ESA of two representative T cell epitopes were also calculated as benchmarks. One is the HLA-A2–M1, a viral antigen “M1” ($M1_{58\text{-}66}$ from the IAV) in complex with HLA-A*02:01(A2-M1, in Fig. 4a), which considered as a featureless epitope[62]. In contrast, a viral epitope HLA-A2-RT, which has a “reverse transcriptase peptide” ($RT_{468\text{-}476}$ from HIV) in complex with HLA-A*02:01(called A2-RT, in Fig. 4a), is considered as largely exposed epitope[63]. After calculation, we found that the mut9m neoantigen has the smallest peptide ESA at 240 $Å^2$, even less than the well-known featureless M1 peptide (251 $Å^2$, in Fig. 4a-c). However, the mut10m neoantigen has relatively large ESA at 317 $Å^2$, which is comparable with the typical largely exposed antigen RT (330 $Å^2$, in Fig. 4a-c). These data suggested that the mut9m provides relatively less SEA than canonical T cell antigens. We thus postulated that the specific TCRs for C08-mut9m may be constrained in patients because of the featureless area available for specific recognition.

Studies have suggested that narrow TCR repertoires can recognize featureless epitope, because of the lack of TCR recognition modes[61,62,64]. To investigate the diversity of KRAS G12D neoantigen specific TCRs in clinical cases, we examined the TCR sequences of the restricted T cell repertoire targeting the C08-mut9m neoepitope (Fig. 4d, patients 3995 and 4095, both expressing HLA-C*08:02)[10,44]. Patient 3995 received ACT targeting KRAS G12D neoantigen and did not response. The transferred RK5 T cell repertoire (T cells expressed the RK5 TCR) was identified to recognize C08-mut9m neoepitope. Patient 4095 received a similar treatment and observed objective tumor regressions. In patient 4095, the RK1, RK3, RK4 T cell repertoires were verified to recognize

the C08-mut9m while the RK2 recognized the C08-mut10m. All four T cell repertoires (RK1, RK3, RK4, RK5) with C08-mut9m restriction were identified biased usage with a public TCR pair (TRAV4/TRBV5-1) across different patients. The length and sequence of these TCRα chains was highly restricted, with the same TCR-V region and "CLVGDxDQAGTALIF" CDR3α motif among the four TCRs (Fig. 4d). The TCRβ chains was also restricted at TCR-V region but showed differences at CDR3β regions. Generally, the CDR1 and CDR2 loops of TCR can recognize the two conserved α-helixes on the MHC, whereas the CDR3 loops mainly interact with the exposed peptide. Moreover, the CDR3β had proved to be the main factor that determines TCR bias (compared with CDR3α) in many cases, due to the greater sequence diversity in TCR repertoire and the extensive contact of peptide region[64]. However, in this case, similar CDR1, CRR2 and CDR3α sequences with C08-mut9m restriction were identified consistently from different patients. We thus speculation that these public CDR1, CRR2 and CDR3α regions are important in the C08-mut9m recognition, rather than the CDR3β regions[65]. In contrast, the C08-mut10m neoepitope did not observe dominant public TCRs in patient 4095 or across different individuals. Collectively, these data suggested that the featureless mut9m neoepitope can be recognized by T cells with public TCRs across different patients.

Previous reports have shown that the constrained TCR repertoires are associated with poor efficient to control viral infection[66,67]. However, the correlation between TCR bias and clinical outcome in cancer treatment is unclear. In an exploratory analysis, we examined the TCR bias and clinical performance in this case to address above question. The C08-mut9m restricted T cell repertoires with public TCR usage (RK1, RK3 RK4 and RK5) did not dominant presence in TILs or not show long-term persistence after infusion (Fig. 4d, detected after 39 and 266 days). However, the RK2 T cells with C08-mut10m restriction showed dominant persistent abilities both in tumor infiltrating stage and after cell transfer for 266 days. While we did not observe direct correlation between TCR diversity and clinical outcome due to the limitations of clinical data, we still observed short-lived T cell persistence in the presence of the featureless C08-mut9m neoepitope. This phenomenon might be explained due to the existence of cross-reactivity with self antigen and thereby leads to the suppression by regulatory effectors *in vivo*. We thus postulated that, outcomes of patients who receive more diverse adoptive T cells tended to be better than patients who receive constrained T cells in cancer immunotherapy.

Discussion

How the T cells recognize neoantigen as “non-self” is an important question in cancer immunotherapy. In contrast to conventional pathogenic peptides that may totally different from self peptides, the neoantigens are single amino acid altered peptides compare with self peptides. Thus, differences between neoantigens and their wild-type counterparts and how neoantigen-MHC binding events involve in forming new TCR binding surface should be elucidated in neoantigen immunogenicity studies.

Efforts have devoted to discuss the complexity of neoantigen immunogenicity with their binding events. Different pieces of evidence led to different conclusions[68]. Fritsch *et al*. and Yadav *et al*. suggest that neoantigen are more commonly mutated at TCR-contacting position, however, Duan *et al*. thought that neoantigen substitutions at anchor may be more immunogenic[7,18,28]. Further, using mouse model, Capietto *et al*. showed that where the mutation is at an anchor residue, increased affinity relative to the corresponding wild-type peptide can influence neoantigen immunogenicity[29]. To elucidate the questions above, we assigned human neoantigen/neopeptide data into three different categories: mutations at TCR-contacting positions, mutations at MHC-contacting regions but not anchor positions and mutations at anchor positions. In our study, mutations occur more frequently at TCR-contacting positions rather than at MHC-contacting position in immunogenic dataset. It is possible that mutation characteristics, amino acid contact potentials and force-dependent interactions may affect the interactions in the TCR-contacting group[69,70]. For anchor mutated group, we showed that the NP rule in anchor mutated neoantigen is a more pervasive element of immunogenicity than previously understood. Also, we found the NP rule combined with binding predictor (NetMHCpan 4.0) that could contribute to prioritize neoantigen candidates. In a sense, the NP rule could be taken as a reflection of antigen binding property. This binary indicator can provide a direct understanding of the MHC binding difference between mutant peptides and their wild type counterparts. However, the uniqueness of the NP rule was not fully determined, since the test depends on how comprehensive the validation database is. More analyses to understand the NP rule are still needed with the data increasing.

We next performed structural studies to understand the NP rule. The molecular insight of anchor mutated neoantigens provided evidences that they can generate new surface and features for T cell

recognition but the wild-type cannot. In contrast, the anchor mutated neopeptides with PP rule reveal low immunogenicity in clinical treatment, reflecting that the most neoepitope restricted T cells might have been removed by negative selection. It also suggested that neoantigen exposed surface area (ESA) might be a factor to influence TCR diversity and clinical outcome based on our analysis. More experimental data and neoantigen-MHC structures are needed to fully understand the relevance of ESA and TCR diversity.

Our study showed three possible neoantigen binding models within the context of MHC (Supplementary Fig. 4). Model A represents the situation which mutation occurs at the TCR-contacting region and therefore directly towards to T cells. Model B represents the situation in which mutation occurs at MHC-contacting region (not including anchor sites) and therefore might be immunogenically irrelevant. Model C represents the situation which the mutation occurs at an anchor position. Anchor mutations may not change TCR-contacting surface but instead lead to de novo presentation. If the wild type allele prevented presentation in the thymus, self-reactive T cells would not have been selected against.

KRAS G12D mutations is indicative of poor prognosis with negative/poor response to standard cancer treatment. It is one of the most infamous driver mutations target leads to oncogenesis[71]. The neoantigen KRAS G12D in complex with HLA-C*08:02 is a typical case of a human driver mutation derived neoantigen-MHC structure which has been linked to clinical benefits. With these structures, further research could be undertaken to heighten the immunogenicity and stability of KRAS G12D-C*08:02 neoepitope, by taking modification of agonist peptides or by screening non-natural synthetic epitopes[72,73]. Alternatively, our structures could be used to design artificial receptors that bind mutant KRAS peptides based on synthetic biology means. Our findings reveal that immune-based classification is essential for neoantigen immunogenicity study The NP rule, which found in anchor mutated neoantigens, can be used to prioritize neoantigens. Further structural analyses indicated that newly generated surface as well as the ESA in neoantigens affected T cell activation and clinical outcome, suggesting that these factors could be considered in neoantigen discovery and design of future clinical trials.

Materials and Methods

Noneffective neopeptides dataset (NND) generation

In order to generate a minimal noneffective neopeptide dataset, binding prediction was done by NetMHCpan 4.0 Server[24] based on the data from noneffective neopeptide dataset (NND). Different length of mutant peptides from NND were input in NetMHCpan 4.0 Server with custom python scripts. The mutant peptides in 9- or 10-mer length with recommend cut-off (affinity < 500 nM) based on NetMHCpan 4.0 Server were considered to be binders and recorded in the Supplementary Table 3.

Differential agretopic index (DAI) score calculation

The calculation of DAI was described previously[74]. Briefly, peptide binding affinity with HLA was predicted for mutant and wildtype peptide pairs by NetMHCpan 4.0. The DAI score of each neoantigen pair was calculated by subtraction of its predicted IC50 binding affinity from the corresponding wild type counterparts.

Receiver operating characteristic (ROC) curve generation

The AUC value (the area under the ROC Curve) was calculated based on the different predictors listed. The ROC curve was plotted from the false positive rate (FPR) and true positive rate (TPR) values calculated by varying the cut-off value (separating the predicted positive from the predicted negative) from high to low.

Anchor, MHC-contacting and TCR-contacting positions determination

Identification of the anchor positions were based on the SYFPEITHI online database[56] and manually defined from NetMHCpan binding motif results[24]. Anchors were defined for each allele with the SYFPEITHI database definition and highest information content in NetMHCpan binding motif record. The anchor position for each entry was cross-validated based on solved HLA structures from Protein Data Bank (PDB). Thus, the combination of these tools can provide anchor position information for most HLA alleles in our datasets. We recorded the cross-validated result as the “consensus anchor”. The anchor position information was also recorded in IND and NND. Alleles without relevant

information above were recorded as “null” in the tables.

Peptide MHC-contacting and TCR-contacting positions was determined based on solved 9mer peptide-MHC complex. Briefly, positions from peptides which prove to be non-anchor position can be divided into MHC-contacting and TCR-contacting positions. With the pMHC structural model from PDB, the position on peptide which contact MHC was treated as MHC-contacting position. Contrary to MHC-contacting position, TCR-contacting position often harbor a residue with a side chain that points toward outside from the pMHC complex and may contact with TCR. The MHC contact and TCR contact region information was recorded in IND and NND. Alleles without relevant structure information above were recorded as “null” in the tables.

Peptide library and preferential HLA anchor position determination

The nonameric peptide library of 30 HLA alleles was obtained from IEDB database[58]. Sequence logos were generated base using the sequence logo generator[75]. Threshold for preferential amino acids at anchor position of each HLA alleles was set to include and above 10% based on the data from nonameric peptide library. Preferential information of amino acids at anchor position for each HLA allele was recorded in Supplementary Table 1 and 3.

Combined NP+Binding (Con NP+B) prediction model building

To combined the binary NP rule with existing prediction methods NetMHCpan 4.0, we took a logistic regression algorithm to model the prediction of immunogenicity. Analyses were performed using the R build-in function glm(), as below:

$$\text{immunogenicity} \sim \text{NP} + \text{Binding prediction}.$$

Anchor mutated neoantigen data was selected to train the model. After fitting, the performance of this model was shown by ROC curve.

To further test this model, we used 50 times resampling. Random resampling of the data (2/3rd resampling) was used for training. The AUC values were calculated by plotROC package. After iteration, the differences of AUC between four models were measured using paired t test in R software.

Protein Expression, refolding and purification

Inclusion bodies of HLA heavy chains and β2M was expressed as described previously[76]. Briefly, The DNA encoding MHC heavy chain (HLA-C*08:02, HLA-C*05:01 and H-2 Kb) and light chain (human β2M and mouse β2M) were synthesized (Idobio) and cloned into pET-22(b) vector (Novagen). The vectors were transformed into the E. coli strain BL21 DE3 (Novagen). Transformants were selected fromand selected on Lurian broth (LB) agar plates containing ampicillin. A single colony was selected and cultured in LB fluid medium with the antibiotics listed above at 37°C. Upon reaching an optical density OD600 of 0.6, expression was induced with the addition of 1mM IPTG. Incubation continued at 37°C for 5h. The cells were harvested by centrifugation and then resuspended in PBS buffer with 1 mM PMSF at 4°C. The cells were lysed, and the lysate was clarified by centrifugation at 10,000 g to collect inclusion bodies. Inclusion bodies were harvested and solubilized in 20 mM Tris (Vetec) pH 8.0, 8 M urea (Vetec), 1 mM EDTA (BBI life sciences), 1 mM DTT (Sinopharm chemical reagent) and 0.2 mM PMSF (Sinopharm chemical reagent).

Refolding was performed in the presence of MHC heavy chain, β2M and peptides as described previously[77]. Briefly, the resolubilized heavy chain (60 mg each) and light chain (25 mg each) in the presence of the corresponding peptide were added into 1 liter of refolding buffer [100 mM Tris (pH 8.4), 0.5 mM oxidized glutathione (BBI life sciences), 5 mM reduced glutathione (BBI life sciences), 400mM L-arginine (Vetec), 2mM EDTA (BBI life sciences)]. After 48h of refolding, the 1 L mixture was transferred into dialysis bag (Spectra) and dialyzed against 15 liters of 10 mM Tris buffer (pH 8.0) at 4□ for 24h.

Refolded proteins were purified by anion exchange chromatography with Q Sepharose HP (GE Healthcare) column then Mono Q column (GE Healthcare) and concentrated by tangential flow filtration using Amicon Ultra centrifugal filters (Merck). For desalination and purification, samples were loaded onto a Superdex 200 increase 10/300 GL column (GE Healthcare) for size exclusion chromatography. Chromatography was taken with BioLogic DuoFlow system (Bio-rad) at a flow rate of 1 ml/min. Peak analysis was performed using the ASTRA software package (BioLogic Chromatography Systems).

Crystallization, data collection, and processing

Purified pMHC complex were concentrated to 10 mg/ml for crystallization trials prior to screening using a series of kits from Hampton Research. Protein complex were crystalized by sitting drop vapor diffusion technique at 4 °C. Single crystals of C08-mut9m and C08-mut10m were obtained in the condition of 0.2 M ammonium acetate, 0.1 M HEPES (pH 6.5), 25% w/v polyethylene glycol 3,350. For the H-2 Kb complex, single crystal of Kb-8mV and Kb-8mL complex were obtained when 4% v/v Tacsimate (pH 6.0), 12% w/v Polyethylene glycol 3,350 was used as the reservoir buffer.

Crystals were transferred to crystallization buffer containing 20% (w/v) glycerol and flash-cooled in liquid nitrogen immediately. The diffraction data were collected at the Shanghai Synchrotron Radiation Facility (Shanghai, China) on beam line BL17U1/BL18U1/BL19U1, and processed using the iMosflm program[78]. Data reduction was performed with Aimless and Pointless in the CCP4 software suite[79]. All structures were determined by molecular replacement using Phaser[80]. The models from the molecular replacement were built using the COOT (Crystallographic Object-Oriented Toolkit) program[81] and subsequently subjected to refinement using Phenix software[82]. Data collection, processing, and refinement statistics are summarized in (Supplementary Table 5). All the structural figures were prepared using PyMOL (http://www.pymol.org) program. The atomic coordinates and structure factors for the reported crystal structures have been deposited on the Protein Data Bank (PDB; http://www.rcsb.org/pdb/).

Acknowledgements

We thank the staff from BL17U1/BL18U1/BL19U1 beamline of National Center for Protein Sciences Shanghai (NCPSS) at Shanghai Synchrotron Radiation Facility, for assistance during crystal data collection. We would like to thank Dr. Eric Tran (Providence Cancer Institute, USA) for his helpful comments and thank Chang-yi Ma (The Chinese University of Hong Kong, China) for advices on data analysis. This research was funded by the National Institutes of Health Grants AI018785 and AI135374 (to P.M.); the National Natural Science Foundation of China 31870728 and 31470738 (to L.Y.); the National Basic Research Program of China 2014CB910103 (to L.Y.); the Science Foundation of Wuhan University 2042016kf0169 (to L.Y.).

Author contributions

P.B., L.Y., and P.M. designed all the experiments; P.B. performed all experiments; P.B. collected neoantigen data; P.B., L.Y., P.M., J.W.K., M.W., Y.L., Y.Z., S.K.C., and J.X. analyzed neoantigen data; P.B., and Q.Z. determined crystal structures; P.B., L.Y., and P.W. analyzed crystal structures; P.B., L.Y., P.M., J.W.K., and S.K.C. wrote the manuscript.

Competing interests

The authors declare that they have no conflict of interest.

References

[1] Vesely MD, Kershaw MH, Schreiber RD, Smyth MJ. Natural Innate and Adaptive Immunity to Cancer. Annu Rev Immunol 2011;29:235–71. https://doi.org/10.1146/annurev-immunol-031210-101324.

[2] Sykulev Y, Joo M, Vturina I, Tsomides TJ, Eisen HN. Evidence that a Single Peptide–MHC Complex on a Target Cell Can Elicit a Cytolytic T Cell Response. Immunity 1996;4:565–71. https://doi.org/10.1016/S1074-7613(00)80483-5.

[3] Tumeh PC, Harview CL, Yearley JH, Shintaku IP, Taylor EJM, Robert L, et al. PD-1 blockade induces responses by inhibiting adaptive immune resistance. Nature 2014;515:568–71. https://doi.org/10.1038/nature13954.

[4] Schumacher TN, Schreiber RD. Neoantigens in cancer immunotherapy. Science 2015;348:69–74. https://doi.org/10.1126/science.aaa4971.

[5] Rizvi NA, Hellmann MD, Snyder A, Kvistborg P, Makarov V, Havel JJ, et al. Mutational landscape determines sensitivity to PD-1 blockade in non-small cell lung cancer. Science 2015;348:124–8. https://doi.org/10.1126/science.aaa1348.

[6] Wang R-F, Wang HY. Immune targets and neoantigens for cancer immunotherapy and precision medicine. Cell Res 2017;27:11–37. https://doi.org/10.1038/cr.2016.155.

[7] Yadav M, Jhunjhunwala S, Phung QT, Lupardus P, Tanguay J, Bumbaca S, et al. Predicting immunogenic tumour mutations by combining mass spectrometry and exome sequencing. Nature 2014;515:572–6. https://doi.org/10.1038/nature14001.

[8] Coulie PG, Van den Eynde BJ, van der Bruggen P, Boon T. Tumour antigens recognized by T lymphocytes: at the core of cancer immunotherapy. Nat Rev Cancer 2014;14:135–46. https://doi.org/10.1038/nrc3670.

[9] Gascoigne NRJ, Rybakin V, Acuto O, Brzostek J. TCR Signal Strength and T Cell Development. Annu Rev Cell Dev Biol 2016;32:327–48.

515 https://doi.org/10.1146/annurev-cellbio-111315-125324.
516 [10] Tran E, Robbins PF, Lu Y-C, Prickett TD, Gartner JJ, Jia L, et al. T-Cell Transfer Therapy
517 Targeting Mutant KRAS in Cancer. N Engl J Med 2016;375:2255–62.
518 https://doi.org/10.1056/NEJMoa1609279.
519 [11] Ott PA, Hu Z, Keskin DB, Shukla SA, Sun J, Bozym DJ, et al. An immunogenic personal
520 neoantigen vaccine for patients with melanoma. Nature 2017;547:217–21.
521 https://doi.org/10.1038/nature22991.
522 [12] Sahin U, Derhovanessian E, Miller M, Kloke B-P, Simon P, Löwer M, et al. Personalized RNA
523 mutanome vaccines mobilize poly-specific therapeutic immunity against cancer. Nature
524 2017;547:222–6. https://doi.org/10.1038/nature23003.
525 [13] Melief CJM. Precision T-cell therapy targets tumours. Nature 2017;547:165–7.
526 https://doi.org/10.1038/nature23093.
527 [14] Chen F, Zou Z, Du J, Su S, Shao J, Meng F, et al. Neoantigen identification strategies enable
528 personalized immunotherapy in refractory solid tumors. J Clin Invest 2019;129:2056–70.
529 https://doi.org/10.1172/JCI99538.
530 [15] Matsushita H, Vesely MD, Koboldt DC, Rickert CG, Uppaluri R, Magrini VJ, et al. Cancer
531 exome analysis reveals a T-cell-dependent mechanism of cancer immunoediting. Nature
532 2012;482:400–4. https://doi.org/10.1038/nature10755.
533 [16] Robbins PF, Lu Y-C, El-Gamil M, Li YF, Gross C, Gartner J, et al. Mining exomic sequencing
534 data to identify mutated antigens recognized by adoptively transferred tumor-reactive T
535 cells. Nat Med 2013;19:747–52. https://doi.org/10.1038/nm.3161.
536 [17] van Rooij N, van Buuren MM, Philips D, Velds A, Toebes M, Heemskerk B, et al. Tumor
537 Exome Analysis Reveals Neoantigen-Specific T-Cell Reactivity in an Ipilimumab-Responsive
538 Melanoma. J Clin Oncol 2013;31:e439–42. https://doi.org/10.1200/JCO.2012.47.7521.
539 [18] Duan F, Duitama J, Al Seesi S, Ayres CM, Corcelli SA, Pawashe AP, et al. Genomic and
540 bioinformatic profiling of mutational neoepitopes reveals new rules to predict anticancer
541 immunogenicity. J Exp Med 2014;211:2231–48. https://doi.org/10.1084/jem.20141308.
542 [19] Cohen CJ, Gartner JJ, Horovitz-Fried M, Shamalov K, Trebska-McGowan K, Bliskovsky VV, et
543 al. Isolation of neoantigen-specific T cells from tumor and peripheral lymphocytes. J Clin
544 Invest 2015;125:3981–91. https://doi.org/10.1172/JCI82416.
545 [20] Carreno BM, Magrini V, Becker-Hapak M, Kaabinejadian S, Hundal J, Petti AA, et al. A
546 dendritic cell vaccine increases the breadth and diversity of melanoma neoantigen-specific
547 T cells. Science 2015;348:803. https://doi.org/10.1126/science.aaa3828.
548 [21] Stronen E, Toebes M, Kelderman S, van Buuren MM, Yang W, van Rooij N, et al. Targeting of
549 cancer neoantigens with donor-derived T cell receptor repertoires. Science
550 2016;352:1337–41. https://doi.org/10.1126/science.aaf2288.
551 [22] Anagnostou V, Smith KN, Forde PM, Niknafs N, Bhattacharya R, White J, et al. Evolution of
552 Neoantigen Landscape during Immune Checkpoint Blockade in Non–Small Cell Lung Cancer.
553 Cancer Discov 2017;7:264–76. https://doi.org/10.1158/2159-8290.CD-16-0828.
554 [23] Zacharakis N, Chinnasamy H, Black M, Xu H, Lu Y-C, Zheng Z, et al. Immune recognition of
555 somatic mutations leading to complete durable regression in metastatic breast cancer. Nat
556 Med 2018;24:724–30. https://doi.org/10.1038/s41591-018-0040-8.
557 [24] Jurtz VI, Paul S, Andreatta M, Marcatili P, Peters B, Nielsen M. NetMHCpan 4.0: Improved
558 peptide-MHC class I interaction predictions integrating eluted ligand and peptide binding

559 affinity data 2017. https://doi.org/10.1101/149518.
560 [25] Andreatta M, Nielsen M. Gapped sequence alignment using artificial neural networks:
561 application to the MHC class I system. Bioinformatics 2016;32:511–7.
562 https://doi.org/10.1093/bioinformatics/btv639.
563 [26] Vitiello A, Zanetti M. Neoantigen prediction and the need for validation. Nat Biotechnol
564 2017;35:815–7. https://doi.org/10.1038/nbt.3932.
565 [27] Bulik-Sullivan B, Busby J, Palmer CD, Davis MJ, Murphy T, Clark A, et al. Deep learning using
566 tumor HLA peptide mass spectrometry datasets improves neoantigen identification. Nat
567 Biotechnol 2019;37:55–63. https://doi.org/10.1038/nbt.4313.
568 [28] Fritsch EF, Rajasagi M, Ott PA, Brusic V, Hacohen N, Wu CJ. HLA-Binding Properties of Tumor
569 Neoepitopes in Humans. Cancer Immunol Res 2014;2:522–9.
570 https://doi.org/10.1158/2326-6066.CIR-13-0227.
571 [29] Capietto A-H, Jhunjhunwala S, Pollock SB, Lupardus P, Wong J, Hänsch L, et al. Mutation
572 position is an important determinant for predicting cancer neoantigens. J Exp Med
573 2020;217. https://doi.org/10.1084/jem.20190179.
574 [30] Hogan KT, Eisinger DP, Cupp SB, Lekstrom KJ, Deacon DD, Shabanowitz J, et al. The Peptide
575 Recognized by HLA-A68.2-restricted, Squamous Cell Carcinoma of the Lung-specific
576 Cytotoxic T Lymphocytes Is Derived from a Mutated Elongation Factor 2 Gene.
577 Cancer Res 1998;58:5144.
578 [31] McGranahan N, Furness AJS, Rosenthal R, Ramskov S, Lyngaa R, Saini SK, et al. Clonal
579 neoantigens elicit T cell immunoreactivity and sensitivity to immune checkpoint blockade.
580 Science 2016;351:1463–9. https://doi.org/10.1126/science.aaf1490.
581 [32] Robbins PF. A mutated beta-catenin gene encodes a melanoma-specific antigen recognized
582 by tumor infiltrating lymphocytes. J Exp Med 1996;183:1185–92.
583 https://doi.org/10.1084/jem.183.3.1185.
584 [33] Zorn E, Hercend T. A natural cytotoxic T cell response in a spontaneously regressing human
585 melanoma targets a neoantigen resulting from a somatic point mutation. Eur J Immunol
586 1999;29:592–601.
587 https://doi.org/10.1002/(SICI)1521-4141(199902)29:02<592::AID-IMMU592>3.0.CO;2-2.
588 [34] Chiari R, Foury F, De Plaen E, Baurain J-F, Thonnard J, G. Coulie P. Two Antigens Recognized
589 by Autologous Cytolytic T Lymphocytes on a Melanoma Result from a Single Point Mutation
590 in an Essential Housekeeping Gene. Cancer Res 1999;59:5785.
591 [35] Echchakir H, Mami-Chouaib F, Vergnon I, Baurain J-F, Karanikas V, Chouaib S, et al. A Point
592 Mutation in the α-Actinin-4 Gene Generates an Antigenic Peptide Recognized by
593 Autologous Cytolytic T Lymphocytes on a Human Lung Carcinoma. Cancer Res
594 2001;61:4078.
595 [36] Guéguen M, Patard J-J, Gaugler B, Brasseur F, Renauld J-C, Van Cangh PJ, et al. An Antigen
596 Recognized by Autologous CTLs on a Human Bladder Carcinoma. J Immunol 1998;160:6188.
597 [37] Zhou J, Dudley ME, Rosenberg SA, Robbins PF. Persistence of Multiple Tumor-Specific T-Cell
598 Clones Is Associated with Complete Tumor Regression in a Melanoma Patient Receiving
599 Adoptive Cell Transfer Therapy: J Immunother 2005;28:53–62.
600 https://doi.org/10.1097/00002371-200501000-00007.
601 [38] Sensi M, Nicolini G, Zanon M, Colombo C, Molla A, Bersani I, et al. Immunogenicity without
602 Immunoselection: A Mutant but Functional Antioxidant Enzyme Retained in a Human

603 Metastatic Melanoma and Targeted by CD8+ T Cells with a Memory Phenotype. Cancer Res
604 2005:10.
605 [39] Lennerz V, Fatho M, Gentilini C, Frye RA, Lifke A, Ferel D, et al. The response of autologous T
606 cells to a human melanoma is dominated by mutated neoantigens. Proc Natl Acad Sci
607 2005;102:16013–8. https://doi.org/10.1073/pnas.0500090102.
608 [40] Takenoyama M, Baurain J-F, Yasuda M, So T, Sugaya M, Hanagiri T, et al. A point mutation in
609 the NFYC gene generates an antigenic peptide recognized by autologous cytolytic T
610 lymphocytes on a human squamous cell lung carcinoma: NF-YC Mutated Peptide-Reactive
611 CTL in NSCLC. Int J Cancer 2006;118:1992–7. https://doi.org/10.1002/ijc.21594.
612 [41] Ito D, Visus C, Hoffmann TK, Balz V, Bier H, Appella E, et al. Immunological characterization
613 of missense mutations occurring within cytotoxic T cell-defined p53 epitopes in
614 HLA-A*0201+ squamous cell carcinomas of the head and neck. Int J Cancer
615 2007;120:2618–24. https://doi.org/10.1002/ijc.22584.
616 [42] Wick DA, Webb JR, Nielsen JS, Martin SD, Kroeger DR, Milne K, et al. Surveillance of the
617 Tumor Mutanome by T Cells during Progression from Primary to Recurrent Ovarian Cancer.
618 Clin Cancer Res 2014;20:1125–34. https://doi.org/10.1158/1078-0432.CCR-13-2147.
619 [43] Lu Y-C, Yao X, Crystal JS, Li YF, El-Gamil M, Gross C, et al. Efficient Identification of Mutated
620 Cancer Antigens Recognized by T Cells Associated with Durable Tumor Regressions. Clin
621 Cancer Res 2014;20:3401–10. https://doi.org/10.1158/1078-0432.CCR-14-0433.
622 [44] Tran E, Ahmadzadeh M, Lu Y-C, Gros A, Turcotte S, Robbins PF, et al. Immunogenicity of
623 somatic mutations in human gastrointestinal cancers. Science 2015;350:1387–90.
624 https://doi.org/10.1126/science.aad1253.
625 [45] Snyder A, Makarov V, Merghoub T, Yuan J, Zaretsky JM, Desrichard A, et al. Genetic Basis for
626 Clinical Response to CTLA-4 Blockade in Melanoma. N Engl J Med 2014;371:2189–99.
627 https://doi.org/10.1056/NEJMoa1406498.
628 [46] Kalaora S, Wolf Y, Feferman T, Barnea E, Greenstein E, Reshef D, et al. Combined Analysis of
629 Antigen Presentation and T-cell Recognition Reveals Restricted Immune Responses in
630 Melanoma. Cancer Discov 2018;8:1366–75.
631 https://doi.org/10.1158/2159-8290.CD-17-1418.
632 [47] Gros A, Parkhurst MR, Tran E, Pasetto A, Robbins PF, Ilyas S, et al. Prospective identification
633 of neoantigen-specific lymphocytes in the peripheral blood of melanoma patients. Nat Med
634 2016;22:433–8. https://doi.org/10.1038/nm.4051.
635 [48] Prickett TD, Crystal JS, Cohen CJ, Pasetto A, Parkhurst MR, Gartner JJ, et al. Durable
636 Complete Response from Metastatic Melanoma after Transfer of Autologous T Cells
637 Recognizing 10 Mutated Tumor Antigens. Cancer Immunol Res 2016;4:669–78.
638 https://doi.org/10.1158/2326-6066.CIR-15-0215.
639 [49] Parkhurst M, Gros A, Pasetto A, Prickett T, Crystal JS, Robbins P, et al. Isolation of T-Cell
640 Receptors Specifically Reactive with Mutated Tumor-Associated Antigens from
641 Tumor-Infiltrating Lymphocytes Based on CD137 Expression. Clin Cancer Res
642 2017;23:2491–505. https://doi.org/10.1158/1078-0432.CCR-16-2680.
643 [50] Stevanović S, Pasetto A, Helman SR, Gartner JJ, Prickett TD, Howie B, et al. Landscape of
644 immunogenic tumor antigens in successful immunotherapy of virally induced epithelial
645 cancer. Science 2017;356:200–5. https://doi.org/10.1126/science.aak9510.
646 [51] Le DT, Durham JN, Smith KN, Wang H, Bartlett BR, Aulakh LK, et al. Mismatch repair

647 deficiency predicts response of solid tumors to PD-1 blockade. Science 2017;357:409–13.
648 https://doi.org/10.1126/science.aan6733.
649 [52] Deniger DC, Pasetto A, Robbins PF, Gartner JJ, Prickett TD, Paria BC, et al. T-cell Responses
650 to *TP53* "Hotspot" Mutations and Unique Neoantigens Expressed by Human Ovarian
651 Cancers. Clin Cancer Res 2018;24:5562–73.
652 https://doi.org/10.1158/1078-0432.CCR-18-0573.
653 [53] The problem with neoantigen prediction. Nat Biotechnol 2017;35:97–97.
654 https://doi.org/10.1038/nbt.3800.
655 [54] Chen DS, Mellman I. Elements of cancer immunity and the cancer–immune set point.
656 Nature 2017;541:321–30. https://doi.org/10.1038/nature21349.
657 [55] Havel JJ, Chowell D, Chan TA. The evolving landscape of biomarkers for checkpoint inhibitor
658 immunotherapy. Nat Rev Cancer 2019;19:133–50.
659 https://doi.org/10.1038/s41568-019-0116-x.
660 [56] Rammensee H-G, Bachmann J, Emmerich NPN, Bachor OA, Stevanović S. SYFPEITHI:
661 database for MHC ligands and peptide motifs. Immunogenetics 1999;50:213–9.
662 https://doi.org/10.1007/s002510050595.
663 [57] Falk K, Rötzschke O, Stevanovié S, Jung G, Rammensee H-G. Allele-specific motifs revealed
664 by sequencing of self-peptides eluted from MHC molecules. Nature 1991;351:290–6.
665 https://doi.org/10.1038/351290a0.
666 [58] Vita R, Mahajan S, Overton JA, Dhanda SK, Martini S, Cantrell JR, et al. The Immune Epitope
667 Database (IEDB): 2018 update. Nucleic Acids Res 2019;47:D339–43.
668 https://doi.org/10.1093/nar/gky1006.
669 [59] Di Marco M, Schuster H, Backert L, Ghosh M, Rammensee H-G, Stevanović S. Unveiling the
670 Peptide Motifs of HLA-C and HLA-G from Naturally Presented Peptides and Generation of
671 Binding Prediction Matrices. J Immunol 2017:ji1700938.
672 https://doi.org/10.4049/jimmunol.1700938.
673 [60] Davis MM. The problem of plain vanilla peptides. Nat Immunol 2003;4:649–50.
674 https://doi.org/10.1038/ni0703-649.
675 [61] Song I, Gil A, Mishra R, Ghersi D, Selin LK, Stern LJ. Broad TCR repertoire and diverse
676 structural solutions for recognition of an immunodominant CD8+ T cell epitope. Nat Struct
677 Mol Biol 2017;24:395–406. https://doi.org/10.1038/nsmb.3383.
678 [62] Stewart-Jones GBE, McMichael AJ, Bell JI, Stuart DI, Jones EY. A structural basis for
679 immunodominant human T cell receptor recognition. Nat Immunol 2003;4:7.
680 [63] Celie PHN, Toebes M, Rodenko B, Ovaa H, Perrakis A, Schumacher TNM. UV-Induced Ligand
681 Exchange in MHC Class I Protein Crystals. J Am Chem Soc 2009;131:12298–304.
682 https://doi.org/10.1021/ja9037559.
683 [64] Turner SJ, Doherty PC, McCluskey J, Rossjohn J. Structural determinants of T-cell receptor
684 bias in immunity. Nat Rev Immunol 2006;6:883–94. https://doi.org/10.1038/nri1977.
685 [65] Rudolph MG, Stanfield RL, Wilson IA. HOW TCRS BIND MHCS, PEPTIDES, AND
686 CORECEPTORS. Annu Rev Immunol 2006;24:419–66.
687 https://doi.org/10.1146/annurev.immunol.23.021704.115658.
688 [66] Wang GC, Dash P, McCullers JA, Doherty PC, Thomas PG. T Cell Receptor αβ Diversity
689 Inversely Correlates with Pathogen-Specific Antibody Levels in Human Cytomegalovirus
690 Infection. Sci Transl Med 2012;4:128ra42. https://doi.org/10.1126/scitranslmed.3003647.

691 [67] Yager EJ, Ahmed M, Lanzer K, Randall TD, Woodland DL, Blackman MA. Age-associated
692 decline in T cell repertoire diversity leads to holes in the repertoire and impaired immunity
693 to influenza virus. J Exp Med 2008;205:711–23. https://doi.org/10.1084/jem.20071140.
694 [68] Yarchoan M, Johnson BA, Lutz ER, Laheru DA, Jaffee EM. Targeting neoantigens to augment
695 antitumour immunity. Nat Rev Cancer 2017;17:209–22.
696 https://doi.org/10.1038/nrc.2016.154.
697 [69] Kawashima S, Pokarowski P, Pokarowska M, Kolinski A, Katayama T, Kanehisa M. AAindex:
698 amino acid index database, progress report 2008. Nucleic Acids Res 2007;36:D202–5.
699 https://doi.org/10.1093/nar/gkm998.
700 [70] Sibener LV, Fernandes RA, Kolawole EM, Carbone CB, Liu F, McAffee D, et al. Isolation of a
701 Structural Mechanism for Uncoupling T Cell Receptor Signaling from Peptide-MHC Binding.
702 Cell 2018;174:672-687.e27. https://doi.org/10.1016/j.cell.2018.06.017.
703 [71] June CH. Drugging the Undruggable Ras — Immunotherapy to the Rescue? N Engl J Med
704 2016;375:2286–9. https://doi.org/10.1056/NEJMe1612215.
705 [72] Chen J-L, Stewart-Jones G, Bossi G, Lissin NM, Wooldridge L, Choi EML, et al. Structural and
706 kinetic basis for heightened immunogenicity of T cell vaccines. J Exp Med
707 2005;201:1243–55. https://doi.org/10.1084/jem.20042323.
708 [73] Miles JJ, Tan MP, Dolton G, Edwards ESJ, Galloway SAE, Laugel B, et al. Peptide mimic for
709 influenza vaccination using nonnatural combinatorial chemistry. J Clin Invest
710 2018;128:1569–80. https://doi.org/10.1172/JCI91512.
711 [74] Ghorani E, Rosenthal R, McGranahan N, Reading JL, Lynch M, Peggs KS, et al. Differential
712 binding affinity of mutated peptides for MHC class I is a predictor of survival in advanced
713 lung cancer and melanoma. Ann Oncol 2018;29:271–9.
714 https://doi.org/10.1093/annonc/mdx687.
715 [75] Thomsen MCF, Nielsen M. Seq2Logo: a method for construction and visualization of amino
716 acid binding motifs and sequence profiles including sequence weighting, pseudo counts
717 and two-sided representation of amino acid enrichment and depletion. Nucleic Acids Res
718 2012;40:W281–7. https://doi.org/10.1093/nar/gks469.
719 [76] Yin L, Huseby E, Scott-Browne J, Rubtsova K, Pinilla C, Crawford F, et al. A Single T Cell
720 Receptor Bound to Major Histocompatibility Complex Class I and Class II Glycoproteins
721 Reveals Switchable TCR Conformers. Immunity 2011;35:23–33.
722 https://doi.org/10.1016/j.immuni.2011.04.017.
723 [77] Macdonald WA, Chen Z, Gras S, Archbold JK, Tynan FE, Clements CS, et al. T Cell
724 Allorecognition via Molecular Mimicry. Immunity 2009;31:897–908.
725 https://doi.org/10.1016/j.immuni.2009.09.025.
726 [78] Battye TGG, Kontogiannis L, Johnson O, Powell HR, Leslie AGW. *iMOSFLM*: a new graphical
727 interface for diffraction-image processing with *MOSFLM*. Acta Crystallogr D Biol Crystallogr
728 2011;67:271–81. https://doi.org/10.1107/S0907444910048675.
729 [79] Winn MD, Ballard CC, Cowtan KD, Dodson EJ, Emsley P, Evans PR, et al. Overview of the *CCP*
730 4 suite and current developments. Acta Crystallogr D Biol Crystallogr 2011;67:235–42.
731 https://doi.org/10.1107/S0907444910045749.
732 [80] McCoy AJ, Grosse-Kunstleve RW, Adams PD, Winn MD, Storoni LC, Read RJ. *Phaser*
733 crystallographic software. J Appl Crystallogr 2007;40:658–74.
734 https://doi.org/10.1107/S0021889807021206.

[81] Emsley P, Cowtan K. *Coot*: model-building tools for molecular graphics. Acta Crystallogr D Biol Crystallogr 2004;60:2126–32. https://doi.org/10.1107/S0907444904019158.

[82] Adams PD, Grosse-Kunstleve RW, Hung L-W, Ioerger TR, McCoy AJ, Moriarty NW, et al. *PHENIX*: building new software for automated crystallographic structure determination. Acta Crystallogr D Biol Crystallogr 2002;58:1948–54. https://doi.org/10.1107/S0907444902016657.

Figure 1

a

	Immunogenic Neoantigen Dataset (IND)	Raw Noneffective Neopeptide Dataset (RNND)	Noneffective Neoantigen Dataset (NND)
Entries	128	11,739	2,883
Anchor Mutated Peptides	29	N	428
Tumor Types	15	11	10
HLA-A	14	15	15
HLA-B	14	20	17
HLA-C	7	15	13
Genes	105	1,929	1,081
References	34	13	11

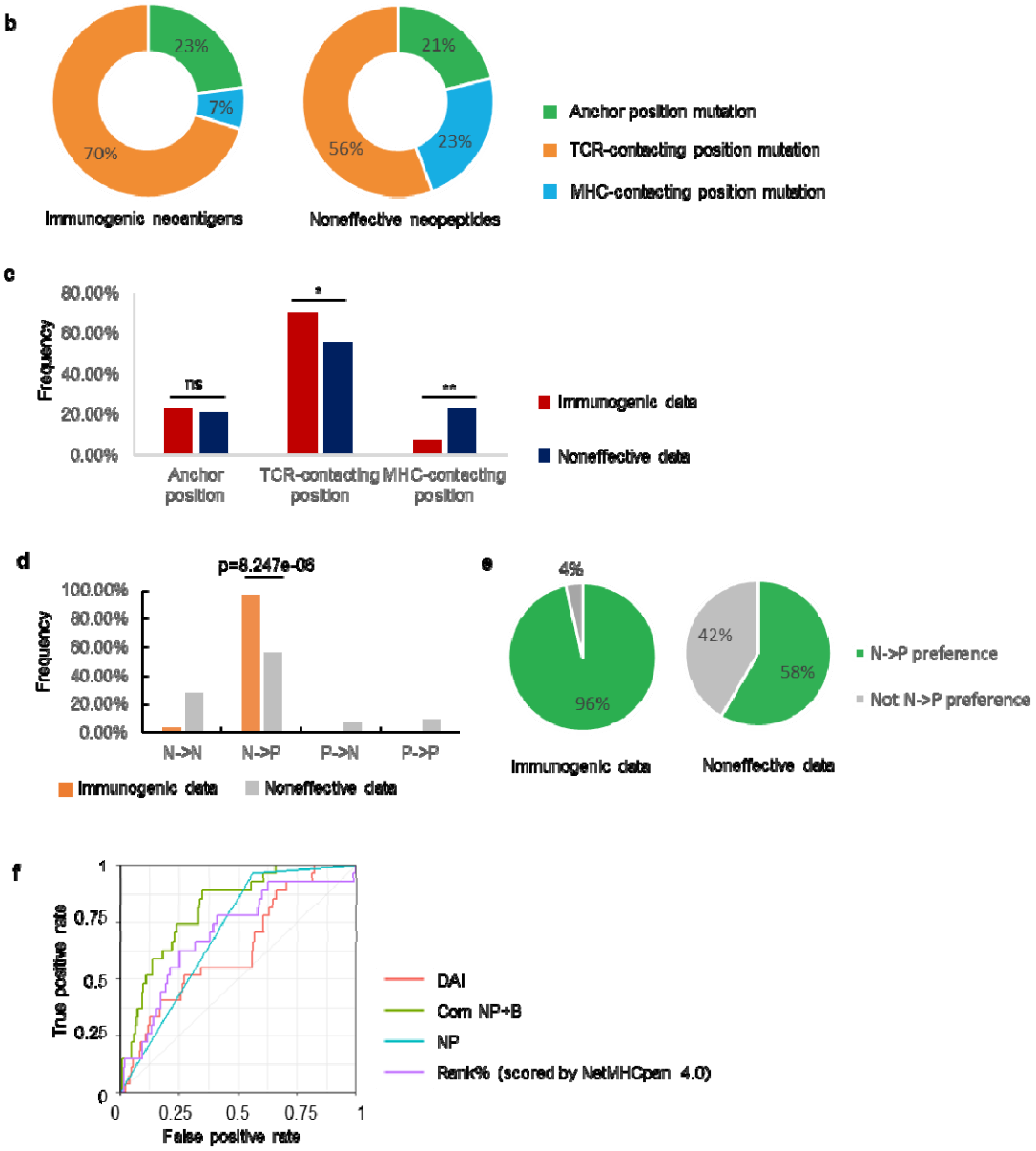

Figure 2

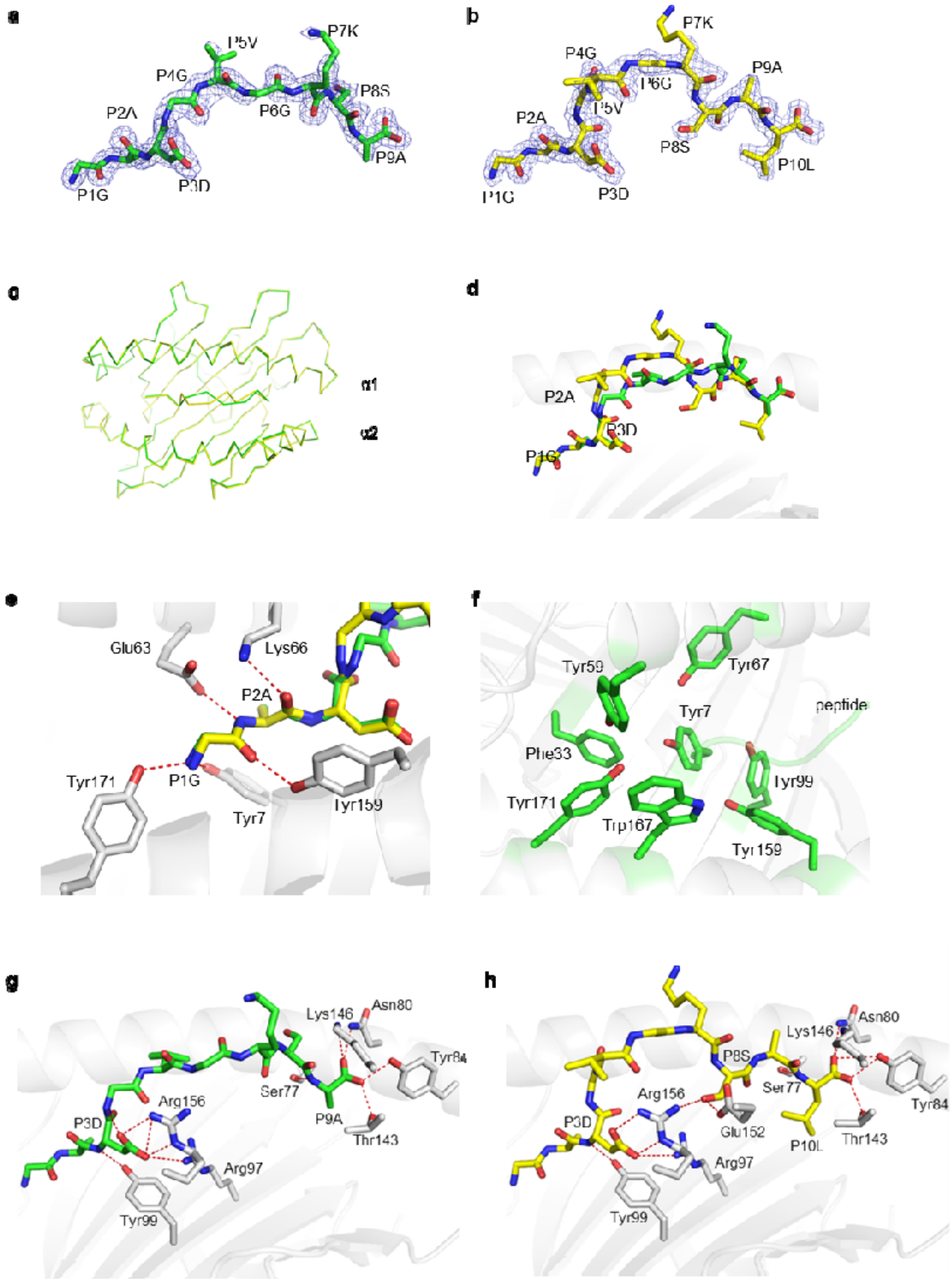
a
P7K
P5V
P4G
P8S
P2A
P6G
P9A
P1G
P3D
b
P7K
P4G
P9A
P6G
P5V
P2A
P8S
P10L
P1G
P3D
c
α1
α2
d
P2A
P3D
P1G
e
Glu63
Lys66
P2A
Tyr171
P1G
Tyr7
Tyr159
f
Tyr59
Tyr67
Tyr7
peptide
Phe33
Tyr99
Tyr171
Trp167
Tyr159
g
Lys146
Asn80
Tyr84
Ser77
Arg156
P3D
P9A
Thr143
Arg97
Tyr99
h
Asn80
Lys146
P8S
Ser77
Arg156
Tyr84
P3D
Glu152
P10L
Thr143
Arg97
Tyr99

Figure 3

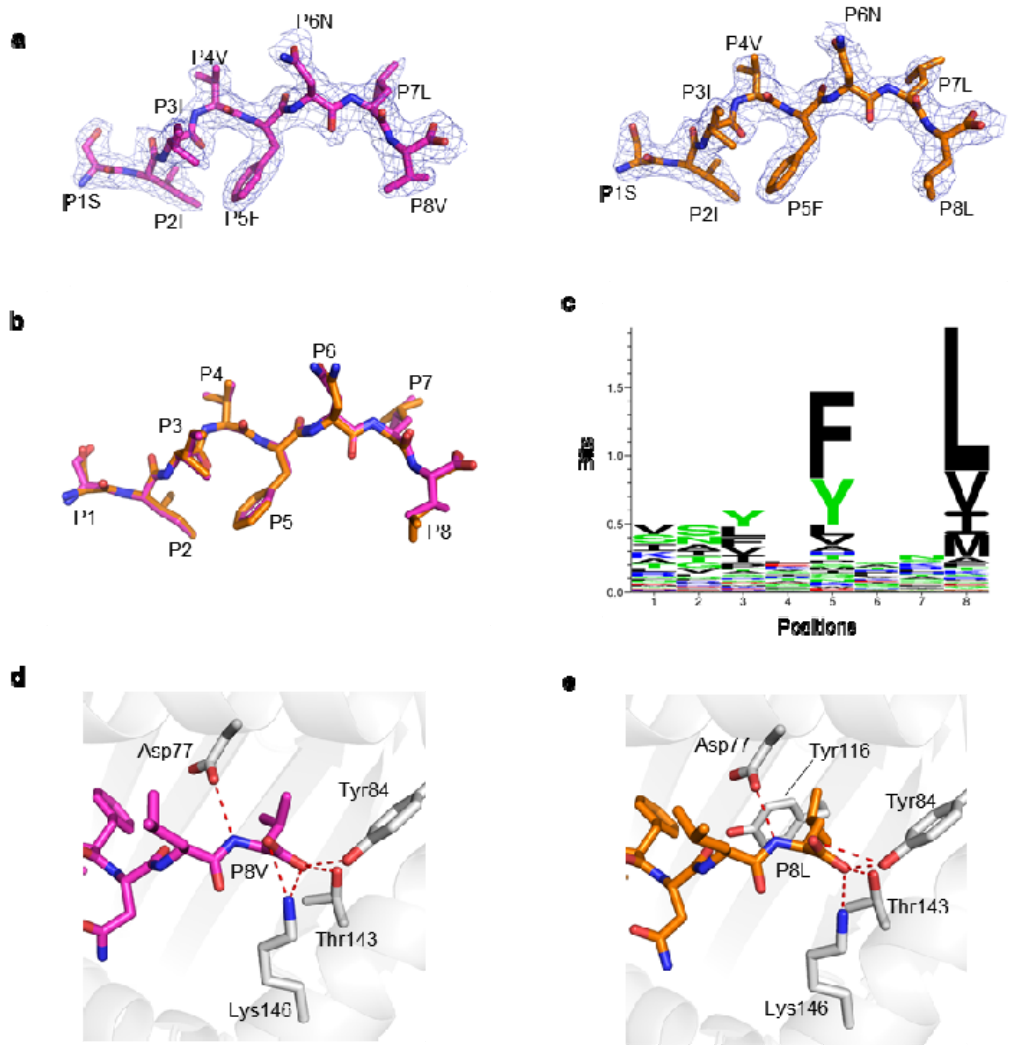
a
P6N
P4V
P3I
P7L
P1S
P2I
P5F
P8V
P6N
P4V
P3I
P7L
P1S
P2I
P5F
P8L
b
P6
P4
P7
P3
P1
P5
P2
P8
c
Bits
Positions
d
Asp77
Tyr84
P8V
Thr143
Lys146
e
Asp77
Tyr116
Tyr84
P8L
Thr143
Lys146

Figure 4

a

pMHC name	Peptide	PESA (Å^2)
C08-mut9m	GADGVGKSA	239.69
C08-mut10m	GADGVGKSAI	318.80
A2-IAV M1	GILGFVFTL	200.80
A2-HIV RT	ILKEPVHGV	329.66

b

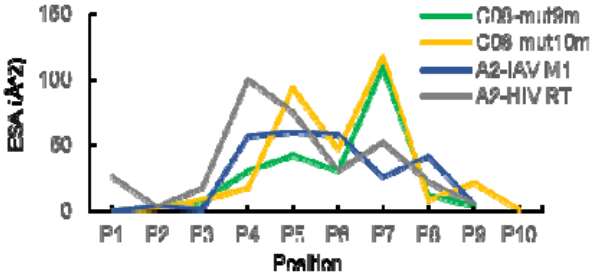

c

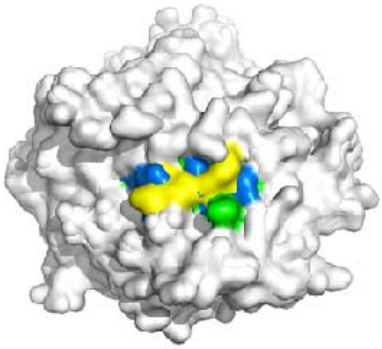

d

Patient ID	TCR Pair Name	TCRα/TCRβ	TCRα/TCRβ CDR3 AA sequence	Rank in Tumor Sample*	Rank in Infusion Product	Rank in Blood
4096	R<1	TRAV4/ TRBV6-6	CLVGDMDQAGTALIF/ CASSLGEGRVDGYTF	20/28/33	1	ND (d+288)
4096	R<2	TRAV12-2/ TRBV10-2	CAAAMDSGYKLIF/ CASSDPGTEAFF	1/1/2	2	1 (d+200)
4096	R<3	TRAV4/ TRBV6-6	CLVGDRDQAGTALIF/ CASSFGQSSTYGYTF	ND	3	5 (d+288)
4096	R<4	TRAV4/ TRBV6-6	CLVGDMDQAGTALIF/ CASSLGRASNGPGHF	917/1306/2243	40	1704 (d+200)
3996	R<5	TRAV4/ TRBV6-6	CLVGDMDQAGTALIF/ CASSLGGTNYGYTF	527	2859	ND (d+39)

Supplementary Figure 1

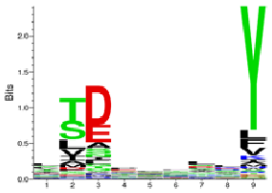

HLA-A*01:01 (n=4661)

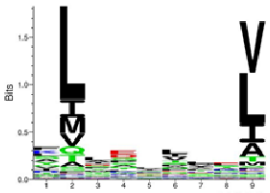

HLA-A*02:01 (n=21172)

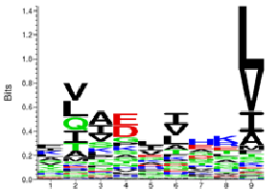

HLA-A*02:05 (n=252)

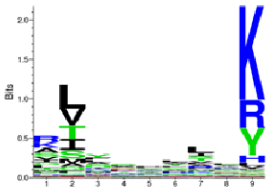

HLA-A*03:01 (n=7487)

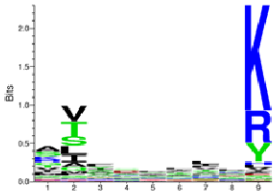

HLA-A*11:01 (n=4850)

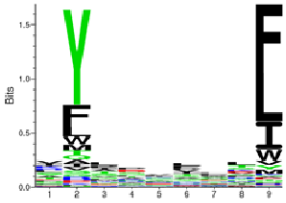

HLA-A*24:02 (n=6683)

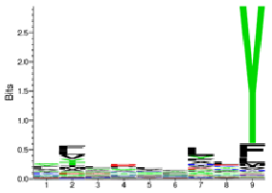

HLA-A*29:02 (n=6009)

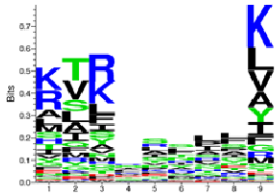

HLA-A*30:01 (n=810)

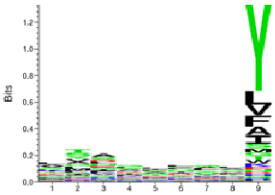

HLA-A*30:02 (n=819)

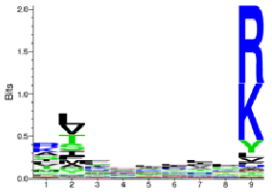

HLA-A*31:01 (n=2000)

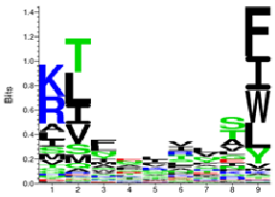

HLA-A*32:01 (n=678)

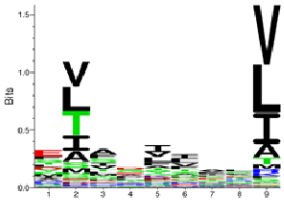

HLA-A*68:02 (n=2995)

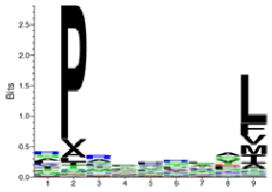

HLA-B*07:02 (n=9573)

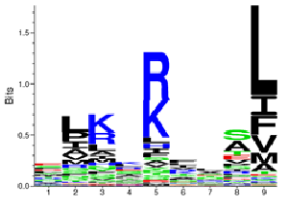

HLA-B*08:01 (n=3955)

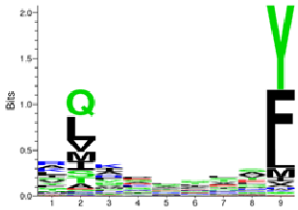

HLA-B*15:01 (n=8349)

(continued on next page)

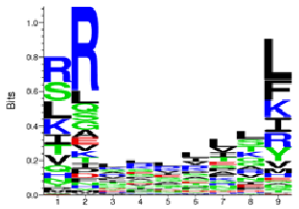

HLA-B*27:05 (n=13590)

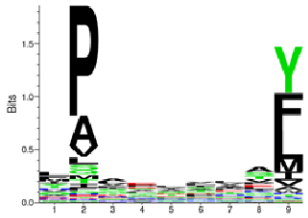

HLA-B*35:01 (n=3023)

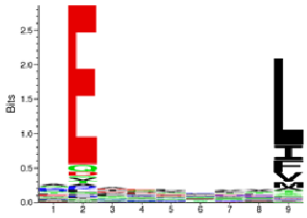

HLA-B*40:01 (n=2148)

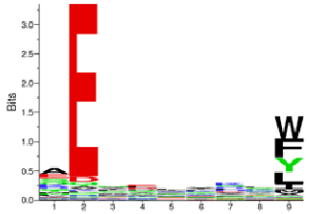

HLA-B*44:02 (n=3531)

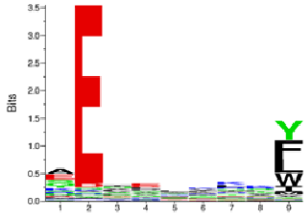

HLA-B*44:03 (n=5166)

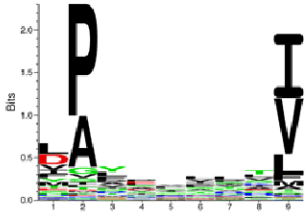

HLA-B*51:01 (n=2869)

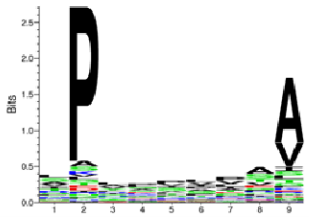

HLA-B*56:01 (n=398)

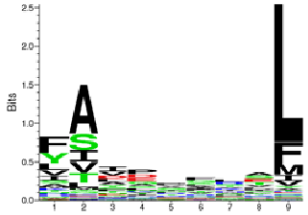

HLA-C*03:03 (n=1020)

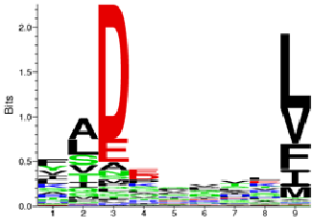

HLA-C*05:01 (n=3251)

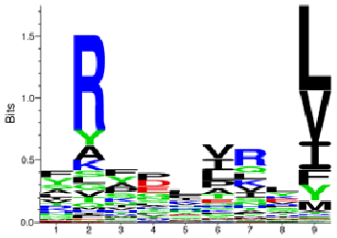

HLA-C*06:02 (n=2069)

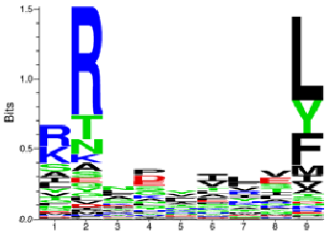

HLA-C*07:01 (n=389)

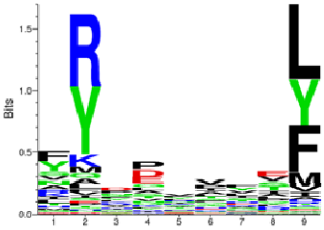

HLA-C*07:02 (n=980)

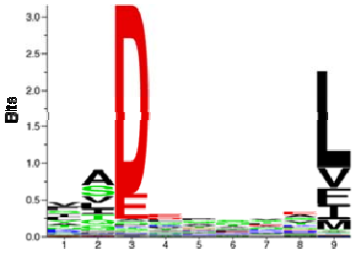

HLA-C*08:02 (n=2321)

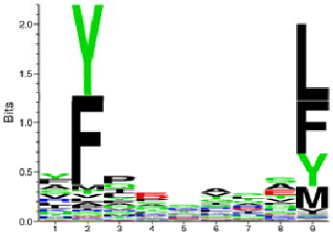

HLA-C*14:02 (n=1899)

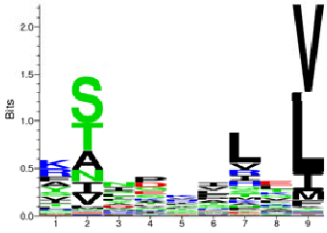

HLA-C*15:02 (n=1747)

Supplementary Figure 2

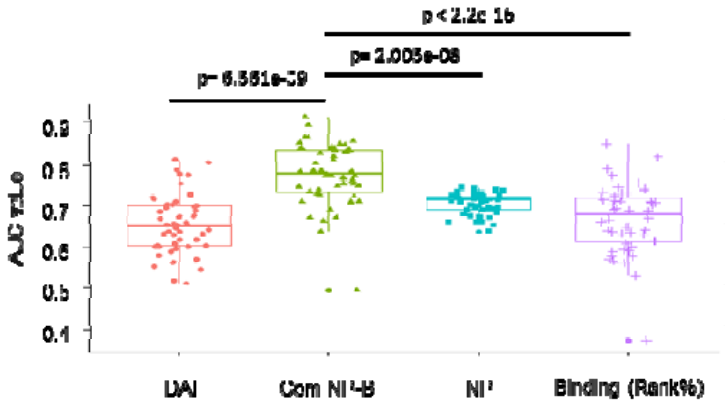

Supplementary Figure 3

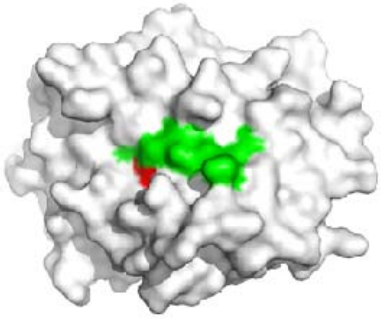

Supplementary Figure 4

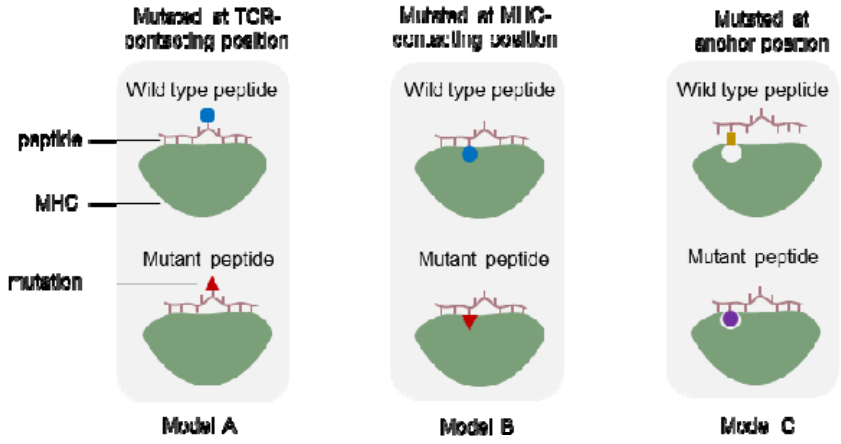

Supplementary Table 1. Immunogenic Neopeptide Dataset (IND)

Supplementary Table 2. Raw Noneffective Neopeptide Dataset (RNND)

Supplementary Table 3. Noneffective Neopeptide Dataset (NND)

(see in separated EXCEL files)

Supplementary Table 4. Classification of anchor mutated neoantigens based on MHC preference

	N->N frequency	N->P frequency	P->N frequency	P->P frequency	Number of peptide
Anchor mutated neoantigens (immunogenic)	3.7% (1)	96.3% (26)	0% (0)	0% (0)	27
Anchor mutated neopeptides (noneffective)	27.76% (118)	56% (238)	6.82% (29)	9.41% (40)	425

Data come from Immunogenic Neoantigen Dataset (IND) and Noneffective Neopeptide Dataset (NND). Peptides defined with anchor position were calculated in this analysis.

Supplementary Table 5. Data collection and refinement statistics (molecular replacement).

	C08-mut9m	C08-mut10m	Kb-8mV	Kb-8mL
Resolution range	42.55 - 1.9 (1.968 - 1.9)	51.13 - [illegible].9 (1.968 - [illegible].9)	57.76 - 2.4 (2.486 - 2.4)	68.67 - 2.5 (2.588 - 2.5)
Space group	P 21 21 21	P 21 21 21	C [illegible] 2 1	C [illegible] 2 [illegible]
Unit cell	68.2796 75.9199 78.0298 90 90 90	68.9397 76.24 78.6998 90 90 90	107.24 69.42 70.4397 90 [illegible]03.79 90	[illegible]06.63 67.9699 70.73 90 [illegible]03.86 90
Total reflections	64768 (6323)	66521 (6583)	37691 (3734)	33008 (3336)
Unique reflections	32450 (3[illegible]74)	33289 (3294)	19013 ([illegible]886)	16646 ([illegible]679)
Multiplicity	2.0 (2.0)	2.0 (2.0)	2.0 (2.0)	2.0 (2.0)
Completeness (%)	0.98 (0.99)	[illegible].00 ([illegible].00)	0.96 (0.96)	0.97 (0.98)
Mean I/sigma(I)	7.15 (4.02)	9.26 (5.12)	14.38 (4.80)	11.90 (2.85)
Wilson B-factor	[illegible]0.39	20.99	38.48	46.2[illegible]
R-merge	0.04092 (0.[illegible]168)	0.03331 (0.1178)	0.02281 (0.1159)	0.02767 (0.1982)
R-meas	0.05787 (0.[illegible]852)	0.04711 (0.1663)	0.03225 (0.1639)	0.039[illegible]3 (0.2803)
CC1/2	0.995 (0.963)	0.998 (0.956)	0.999 (0.979)	0.998 (0.944)
CC*	0.999 (0.99)	0.998 (0.989)	1 (0.995)	1 (0.985)
Reflections used in refinement	31350 (2903)	33285 (3294)	18981 ([illegible]879)	16622 ([illegible]674)
Reflections used for R-free	1936 (155)	2001 (198)	1899 ([illegible]88)	1663 ([illegible]67)
R-work	0.2408	0.174	0.2194	0.2153
R-free	0.2872	0.2044	0.263	0.2934
CC(work)	0.933	0.98	0.943	0.958
CC(free)	0.897	0.949	0.896	0.902
Number of non-hydrogen atoms	3641	3642	3[illegible]52	3093
macromolecules	3127	3139	3044	3045
Protein residues	38[illegible]	382	373	373
RMS(bonds)	0.008	0.007	0.01	0.01
RMS(angles)	0.93	0.93	1.08	1.19
Ramachandran favored (%)	98	99	94	94
Ramachandran allowed (%)	3.2	1.3	5.3	5.1
Ramachandran outliers (%)	0.53	0	0.28	0.85
Rotamer outliers (%)	2.1	1.8	4.3	2.8
Clashscore	8.39	4.9[illegible]	18.38	15.2
Average B-factor	[illegible]7.27	25.67	50.83	59.08
Macromolecules	[illegible]8.15	24.62	50.95	58.2
solvent	24.05	33.81	47.71	61.52

Statistics for the highest-resolution shell are shown in parentheses.

Figure Legends

Figure 1. Analyses of three datasets and immune-based data classification of Immunogenic neoantigen dataset (IND) and Noneffective neopeptides dataset (NND).

a, Overview of the IND, RNND, and NND datasets.

b, Donut plots of percentage of 9mer peptide mutations categorized based on three different mutation locations: anchor mutation, MHC-contacting position and TCR-contacting position (immunogenic data, n =51; noneffective data, n=763).

c, Nonameric peptides mutation distribution of three different groups (mutated at anchor mutation, MHC-contacting position and TCR-contacting position) from IND and NND. The frequency of mutation distribution at TCR-contacting position and MHC-contacting position showed significant difference (TCR-contacting position, p=0.0378; MHC-contacting position, P=0.0027. n (immunogenic) =51; n (noneffective) =763. Fisher's exact test). The percentage of mutation distribution at anchor position did not show significant difference between immunogenic and noneffective data (ns, non-significant).

d, The frequency between anchor mutated IND and NND with significant difference in subgroup of non-preferential to preferential residues (N to P) change (p=8.247e-06, n=27 (immunogenic); n=425 (noneffective), Fisher's exact test). There was no difference between residue changes from wild type neopeptides to different types mutants: non-preferential to non-preferential residues (N to N), preferential to non-preferential residues (P to N) and preferential to preferential residues (P to P)) of anchor mutated immunogenic data (from IND) and non-immunogenic data (from NND).

e, Pie charts represented the percentage of NP group and not NP group of anchor mutated datasets (n (immunogenic) = 27; n (noneffective) =425).

f, Receiver operator characteristic (ROC) curve showed the performance of different predictors (DAI score, binary NP rule, binding prediction (Rank% scored by NetMHCpan 4.0), combination of NP rule + binding prediction (Com NP+B)) with anchor mutated data (data from IND and NND datasets, n (immunogenic) = 27; n (noneffective) =425). The AUC (Area Under the ROC Curve) was calculated for each predictive rule (AUC_{DAI}= 0.632; $AUC_{NP\ rule}$ =0.701; $AUC_{com\ NP\text{-}B}$ =0.810; $AUC_{Rank\%}$=0.698).

Figure 2. Structural comparison of C08-mut9m and C08-mut10m complexes.

a-b, Unambiguous 2Fo-Fc electron density maps of (**a**) KRAS G12D 9mer (GADGVGKSA, green) and (**b**)10mer (GADGVGKSAL, yellow) peptides from solved pMHC complex structures. The underlined amino acids represented the mutation in the peptides.

c, Overlay of Cα traces (C08-mut9m, green; C08-mut10m, yellow). Differences in peptide conformation were observed.

d, Overlay of the KRAS G12D 9mer and 10mer peptides in the MHC binding groove.

e, Polar interactions at P1G and P2A positions within HLA-C*08:02 molecule showed in grey, 9mer peptide showed in green and 10mer peptide showed in yellow.

f, Aromatic residues (green) from HLA-C*08:02 accommodating P1 and P2 residues of KRAS G12D 9mer peptide.

g, The P3D and P9A side chains of mut9m peptide interact with HLA-C*08:02.

h, The P3D, P8S and P10LA side chains of mut10m peptide interact with HLA-C*08:02.

Figure 3. H-2 Kb presented DPAGT V213L wild type peptide wt8mV and mutant peptide mut8mL in a similar manner

a, Unambiguous 2Fo-Fc electron density maps of DPAGT1 wild type 8mer peptide (wt8mV peptide SIIVFNLV, magenta) and mutant 8mer peptide (mut8mL peptide SIIVFNLL, orange) from solved structures.

b, Overlay of the DPAGT1 wt8mV (magenta) and mutant mut8mL (orange) peptides.

c, Sequence logo based on the data from IEDB showing amino acid preferences for 8mer peptides bound to H-2 Kb. The peptide library was obtained from IEDB (n=4141).

d, Anchor residue P8V of wt8mV peptide interacts with H-2 Kb (grey).

e, Anchor residue P8L of mut8mLpeptide interacts with H-2 Kb (grey).

Figure 4. Different peptide presentation patterns and peptide exposed surface areas (PESA) between C08-mut9m and C08-mut10m

a, Peptide exposed surface areas (PESA) of 4 pHLAs. PESA of A2-IAV M1 complex was calculated based on 2VLL (PDB ID). PESA of A2-HIV RT complex was calculated based on 2X4U (PDB ID).

b, Exposed surface areas (ESA) of individual residues at each position of four peptides within HLAs.

c, Mut10m exhibits a relatively large exposed surface area compared to A2-IAV M1 (the featureless benchmark), C08-mut9m and C08-mut10m. HLA backbone surface was shown in grey. IAV M1 (blue), mut9m (green) and mut10m (yellow) peptide surface in different colors.

d, Different T cell fate of KRAS G12D neoantigen restricted T cells reported by previous clinical studies. Rank in tumor sample represents the rank of restricted T cells in patient TILs before cell therapy. Rank in infusion products represents the rank of restricted T cells in ex vivo cell transfer products before cell transfer. Rank in blood represents the rank of restricted T cells in patients' peripheral blood after cell transfer (d+ represents the day after cell transfer). The rank of T cells with same TCR pair was validated in one or three different metastatic tumor fragments from the patient. *, tested in three fragments; †, tested in one fragment; ND, not detected.

Supplementary Figure Legends

Supplementary Figure 1. 9mer peptides binding profile of 30 HLA alleles.

Sequence logos frequent amino acid binding profiles for 9mer peptides bound to each of 30 HLA alleles generated from peptide-binding matrices using the Seq2Logo. Peptide libraries were obtained from IEDB. The sample size of each allele was shown on the figure.

Supplementary Figure 2. The AUC values testing using a 50-fold cross-validation.

The 50-fold cross-validation (2/3rd random resampling) within the exploration set. Differences of AUC values were determined using paired T-test.

Supplementary Figure 3. Additional TCR accessible surface of mut9m neoantigen in complex with HLA-C*08:02.

P3D of C08-mut9m can provide additional TCR accessible surface. HLA-C*08:02 (grey), 9mer peptide (green) and P3D side chain (red) showed in different colors.

Supplementary Figure 4. The topology of different neoantigen-MHC binding models

Model A demonstrates the neoantigens with mutations at TCR-contacting positions that are presented by MHC. The blue circle represents wild type residues. The red triangle represents the mutant residues. Model B demonstrates the neoantigens with mutations at MHC-contacting positions. The red triangle represents the mutant residues compared to the wild type that would affect binding specificity. Model C demonstrates the peptides which have mutations at anchor position and are

presented by MHC. The yellow rectangle represents wild type residues which cannot bind into the anchor position in the MHC peptide presentation groves and thus are not presented. The purple circle represents mutated residues which are preferential selected and bind better at the anchor position.